Solid-State Electronics 90 (2013) 34–38

Contents lists available at SciVerse ScienceDirect

Solid-State Electronics

journal homepage: www.elsevier.com/locate/sse

Subband splitting and surface roughness induced spin relaxation in (001) silicon SOI MOSFETs

Dmitri Osintsev [a,b,*], Oskar Baumgartner [a], Zlatan Stanojevic [a], Viktor Sverdlov [a], Siegfried Selberherr [a]

[a] Institute for Microelectronics, TU Wien, Gußhausstraße 27–29, A–1040 Wien, Austria
[b] Volgograd State Technical University, Lenin Avenue 28, 400131 Volgograd, Russia

ARTICLE INFO

Article history:
Available online 26 March 2013

Keywords:
Thin silicon films
Spin relaxation
$\mathbf{k} \cdot \mathbf{p}$ model
Shear strain

ABSTRACT

Properties of semiconductors provided by the electron spin are of broad interest because of their potential for future spin-driven microelectronic devices. Silicon is the main element of modern charge-based electronics, thus, understanding the details of the spin propagation in silicon structures is key for novel spin-based device application. We use a generalized perturbative $\mathbf{k} \cdot \mathbf{p}$ approach to take the spin degree of freedom into consideration. We investigate (001) oriented SOI films for various parameters including the film thickness, the band offset, and strain. We demonstrate that shear strain dramatically influences the intersubband spin relaxation matrix elements opening a new opportunity to boost spin lifetime in SOI MOSFETs.

© 2013 Elsevier Ltd. All rights reserved.

1. Introduction

Since modern microelectronic devices are nearing their fundamental scaling limits, further boost of their performance could be eventually provided by changing their operation principles. Promising results can be achieved by utilizing the spin properties of electrons. Indeed, the spin of an electron provides two different states (spin-up and spin-down), which could be easily incorporated into the current binary logic. In addition, silicon, being the main material currently used in semiconductor manufacturing, possesses several properties attractive for spin-driven applications: it is composed of nuclei with predominantly zero spin and it is characterized by weak spin–orbit interaction, which should result in a longer spin lifetime as compared to other semiconductors. Spin transfer in silicon over long distances has already been demonstrated experimentally [1]. Spin propagation at such distances combined with a possibility of injecting spin at room [2] or even elevated [3] temperature makes the fabrication of spin-based switching devices quite plausible in the near future. However, the relatively large spin relaxation experimentally observed in electrically-gated lateral-channel silicon structures [4,5] may become an obstacle in realizing spin driven devices [6], and a deeper understanding of fundamental spin relaxation mechanisms in silicon is urgently needed [7].

In this work we investigate the influence of the intrinsic spin–orbit interaction on the subband structure, subband wave functions, and spin relaxation matrix elements due to surface roughness scattering in thin silicon films. Following [6], a $\mathbf{k} \cdot \mathbf{p}$ approach [8,9] suitable to describe the electron subband structure in the presence of strain is generalized to include the spin degree of freedom. In contrast to [6], our effective 4×4 Hamiltonian considers only relevant [001] oriented valleys, with spin included, which produce the low-energy unprimed subband ladder. Without strain the unprimed subbands are degenerate. This degeneracy produces a large mixing between the spin-up and spin-down states, resulting in spin hot spots characterized by strong spin relaxation due to the spin–orbit coupling. These hot spots should be contrasted with the spin hot spots appearing in the bulk system [6,10]. Their origin lies in the unprimed subband degeneracy in a confined electron system and is not related to the degeneracy of the two opposite valleys appearing along certain directions from the *X*-point at the edge of the Brillouin zone. Shear strain is able to efficiently lift the degeneracy between the unprimed subbands [9]. The energy splitting between the otherwise equivalent subbands removes the origin of the spin hot spots in a confined silicon system, which should substantially improve the spin lifetime in gated silicon systems.

2. Method

We investigate numerically the subband splitting, the subband wave functions, and the matrix elements responsible for surface roughness induced scattering and spin relaxation in silicon transistors as a function of shear strain, the silicon film thickness, and the height of the potential barrier at the silicon interface. The film is modeled by a square well potential. The electric field due to the ap-

* Corresponding author at: Institute for Microelectronics, TU Wien, Gußhausstraße 27–29, A–1040 Wien, Austria.
E-mail address: osintsev@iue.tuwien.ac.at (D. Osintsev).

0038-1101/$ - see front matter © 2013 Elsevier Ltd. All rights reserved.
http://dx.doi.org/10.1016/j.sse.2013.02.055

plied gate voltage modulates the bottom of the potential. The dependence of the splitting and the wave functions on the electric field is also investigated. For [001] oriented valleys in a (001) silicon film the Hamiltonian is written in the vicinity of the X point along the k_z-axis in the Brillouin zone. The basis is conveniently chosen as $[(X_1,\uparrow),(X_1,\downarrow),(X_{2'},\uparrow),(X_{2'},\downarrow)]$, where $\uparrow$ and $\downarrow$ indicate the spin projection at the quantization z-axis.

The Hamiltonian is then written as

$$H=\begin{bmatrix} H_1 & H_3 \\ H_3^{\dagger} & H_2 \end{bmatrix} \tag{1}$$

where H_1, H_2, and H_3 are

$$H_j=\left[\frac{\hbar^2 k_z^2}{2m_l}-\frac{(-1)^j\hbar^2 k_0 k_z}{m_l}+\frac{\hbar^2\left(k_x^2+k_y^2\right)}{2m_t}+U(z)\right]I, \tag{2}$$

$$H_3=\begin{bmatrix} D\varepsilon_{xy}-\frac{\hbar^2 k_x k_y}{M} & (k_y-k_x\,\mathrm{i})\varDelta_{so} \\ (-k_y-k_x\,\mathrm{i})\varDelta_{so} & D\varepsilon_{xy}-\frac{\hbar^2 k_x k_y}{M} \end{bmatrix}. \tag{3}$$

Here j = 1,2, I is the identity 2×2 matrix, $U(z)$ is the confinement potential. In the Hamiltonian (1) m_t = 0.19 m_0 and m_l = 0.91m_0 are the transversal and the longitudinal effective masses m_0 is the electron rest mass, k_0 = 0.15 $\times$ $2\pi/a_0$ is the position of the valley minimum relative to the X point in unstrained silicon, ε_{xy} denotes the shear strain component, $M^{-1}\approx m_t^{-1}-m_0^{-1}$, and D = 14 eV is the shear strain deformation potential.

The spin–orbit term $\tau_y\otimes\varDelta_{so}(k_x\sigma_x-k_y\sigma_y)$ with

$$\varDelta_{so}=\frac{\hbar^2}{2m_0^3c^2}\left|\sum_n\frac{\langle X_1|p_j|n\rangle\langle n|[\nabla V\times\mathbf{p}]_j|X_{2'}\rangle}{E_n-E_X}\right|, \tag{4}$$

couples the states with the opposite spin projections from the opposite valleys. In the perturbation theory expression for $\varDelta_{so}$ E_n is the energy of the nth band at the X point, E_X is the energy of the two lowest conduction bands X_1 and X_2' degenerate at the X point, $\mathbf{p}$ is the momentum operator, V is the bulk crystal potential, σ_x, σ_y, and σ_z are the spin Pauli matrices, τ_y is the y-Pauli matrix in the valley degree of freedom and c is the speed of light.

For zero value of the confinement potential the energy dispersion of the lowest conduction bands is given by

$$E(k)=\frac{\hbar^2 k_z^2}{2m_l}+\frac{\hbar^2\left(k_x^2+k_y^2\right)}{2m_t} \pm\sqrt{\left(\frac{\hbar^2 k_z k_0}{m_l}\right)^2+\left(D\varepsilon_{xy}-\frac{\hbar^2 k_x k_y}{M}\right)^2+\varDelta_{so}^2\left(k_x^2+k_y^2\right)}. \tag{5}$$

This expression generalizes the corresponding dispersion relation [6] by including shear strain.

In order to evaluate the strength $\varDelta_{so}$ of the effective spin–orbit interaction we use (5). Close to the X point in the unstrained sample the gap between the X_1 and X_2' conduction bands can be opened by $\varDelta_{so}$ alone if one evaluates the dispersion for $k_x\neq 0$ but k_y = -k_z = 0. The band splitting along the x-axis is then equal to the $2|\varDelta_{so}$-$k_x|$. We used the empirical pseudopotential method (EPM) [9,11] to obtain the splitting numerically. The result is shown in Fig. 1. The dependence on k_x is indeed linear at small values of k_x. By fitting this dependence with a linear function (shown in Fig. 1) at small k_x we found the value $\varDelta_{so}$ = 1.27 meV nm which is close to the one reported in [6].

3. Results and discussion

To find the unprimed subband energies and the eigenfunctions in (001) SOI films we use the Hamiltonian (1) for a numerical solution. We replace k_z with $-i\partial_z$ and we approximate the thin film by a square well with a finite potential barrier corresponding to the film surrounded by a dielectric or another material (Si_xGe_{1-x}/Si/Si_xGe_{1-x} structure, for example) with the same band parameters. The resulting Schrödinger differential equation is discretized along the z-axis and solved using efficient numerical algorithms available through the Vienna Schrödinger–Poisson framework (VSP) [12]. We investigate the two lowest unprimed subbands which are completely equivalent within the effective mass approximation dispersion used to describe each of the [001] valley in the bulk. Because of coupling between the valleys induced by strain and spin–orbit interaction the dispersion (5) becomes non-parabolic. If now a confinement is taken into account, this non-parabolicity results in a pronounced energy splitting between the two lowest otherwise degenerate unprimed subbands.

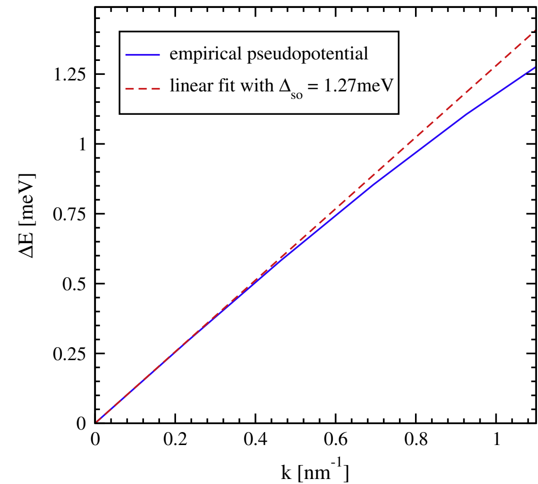

Fig. 1. Empirical pseudopotential calculations of the spin–orbit interaction strength by evaluating the gap opening at the X-point between X_1 and X_2 for finite k_x.

Fig. 2 displays the dependence of the subband splitting on the value of the potential barrier at the silicon interfaces, for shear strain ε_{xy} = 0. For low values of the conduction band offset the subband splitting increases for the considered thicknesses, while we see a saturation at values of the conduction band offset larger than 2 eV, for all thicknesses. The value of the subband splitting at saturation depends strongly on the quantum well thickness. For the 10 nm thick structure the saturation value of the subband splitting

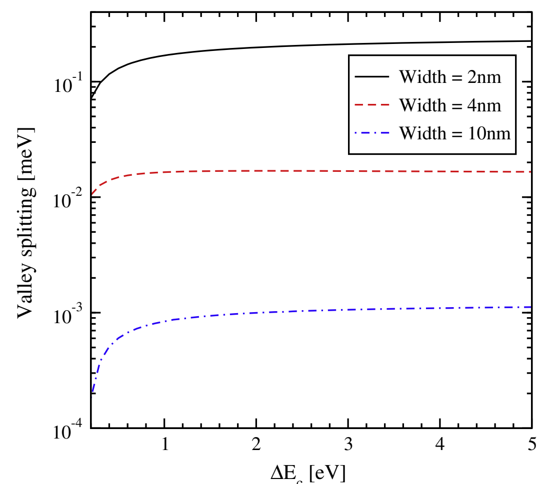

Fig. 2. Splitting between the lowest electron subbands as a function of the conduction band offset at the interface for k_x = 0.25 nm^{-1}, k_y = 0 nm^{-1}, ε_{xy} = 0.

is only 2.3 μeV, while for the quantum well of 4 nm width the splitting saturates at 0.04 meV. For thinner films the saturation value may reach several hundred μeVs.

The subband splitting dependence on the silicon film thickness is analyzed in Fig. 3. Theoretical values for the subband splitting in an infinite potential square well

$$\Delta E = \frac{2y^2 B}{k_0 t\sqrt{(1-y^2-\eta^2)(1-y^2)}} \times \left|\sin\left(\sqrt{\frac{1-y^2-\eta^2}{1-y^2}}k_0 t\right)\right|, \qquad (6)$$

are also shown in Fig. 3 demonstrating good agreement between (6) and $\mathbf{k}\cdot\mathbf{p}$ simulation results. Here $B = \sqrt{\Delta_{so}^2\left(k_x^2+k_y^2\right)+\left(D\varepsilon_{xy}-\frac{\hbar^2 k_x k_y}{M}\right)^2}$, $y = \frac{\pi}{k_0 t}$, $\eta = \frac{m_l B}{k_0^2 \hbar^2}$, and t is the film thickness. To obtain (6) we have generalized the theory [13] for the valley splitting by including the spin–orbit coupling. It is interesting to note, that because the spin–orbit interaction provides coupling between the states with the opposite spin projections but from the opposite valleys, the spin–orbit coupling term in (6) also leads to a subband splitting (lower curve in Fig. 3) in presence of a confining potential. However, because of the two possible ways of coupling the state with spin up (down) from one valley to the spin down (up) state in the opposite valley are allowed, the double-spin degeneracy of the eigenstates is not lifted. This spin degeneracy is preserved in a general case for arbitrary k_x, k_y, when shear strain ε_{xy} is introduced.

The subband splitting oscillates with the film thickness increased (Fig. 3). The value of the subband splitting is drastically enhanced by introducing shear strain. We also note that the period of oscillations depends on strain through $\kappa = \sqrt{\frac{1-y^2-\eta^2}{1-y^2}}k_0$.

The subband splitting as a function of the quantum well width for different values of the effective electric field applied perpendicular to its interface is demonstrated in Fig. 4. Without electric field the subband splitting oscillates as shown in Fig. 4. With the electric field the oscillations are not observed in thicker films. According to Friesen et al. [14] the condition for the independence of the subband splitting from the quantum well width is $t^3 > \frac{2\pi^2\hbar^2}{m_l e E_{field}}$. For thinner structures, the quantization is provided by the second interface barrier of the quantum well, and the shape of the oscillations becomes similar to that in the absence of an electric field. For an electric field of 0.1 MV/cm the quantum well width should be larger than 5.5 nm in order to observe the independence of the subband splitting on the quantum well width. This value is in a good agreement with the simulation results shown in Fig. 4.

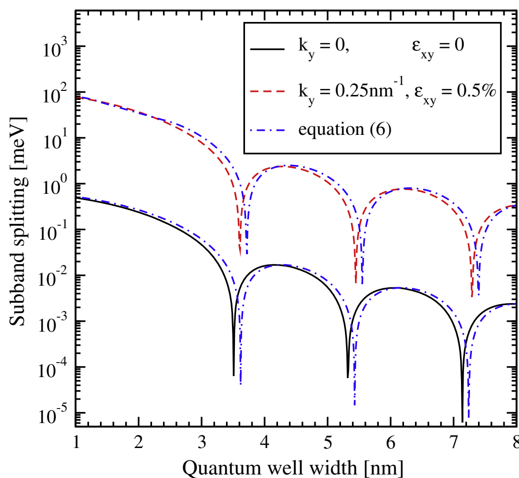

Fig. 3. Splitting of the lowest electron subbands as a function of the silicon film thickness for several values of shear strain and k_y for $k_x = 0.25$ nm^{-1}, $\Delta E_c = 10$ eV.

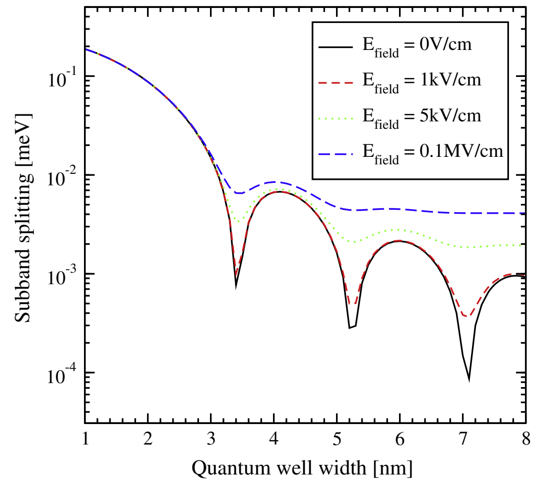

Fig. 4. Splitting of the lowest unprimed electron subbands as a function of the unstrained film thickness for different values of the effective electric field for $k_x = 0.1$ nm^{-1}, $k_y = 0$, $\Delta E_c = 10$ eV.

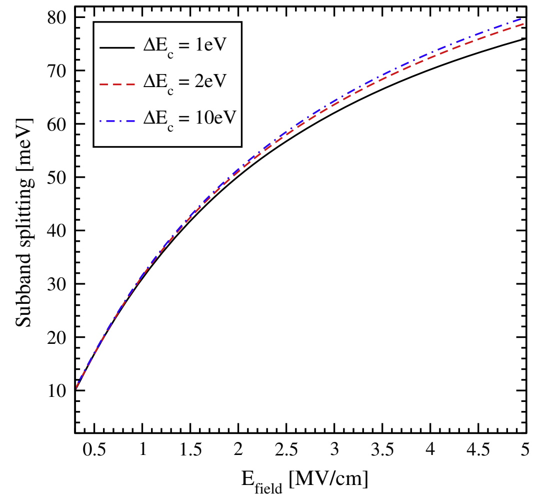

Fig. 5. Subband splitting between the lowest unprimed electron subbands as a function of the electric field, for different conduction band offset values for $k_x = 0.25$ nm^{-1}, $k_y = 0$, $\varepsilon_{xy} = 0.5\%$, $t = 4$ nm.

Fig. 5 shows the subband splitting as a function of the electric field in a thick film (when the splitting does not depend on the film thickness). The shape of the well is triangular and the quantization is provided not by the conduction band offset at the second interface but by the linear potential due to electric field. This is the reason, why for small values of the electric field, no significant difference in the splitting is observed. For large electric field, however, the subband energies are pushed up closer to the edge of the potential well and become comparable to the conduction band offset barrier. This results in a lower subband splitting for smaller values of the effective field. This result is also in agreement with that shown in Fig. 2 indicating that the subband splitting is always smaller for smaller values of the potential barrier at the interface.

Fig. 6 shows the dependence of the subband splitting on the value of shear strain in a 4 nm thick film. Without electric field thesubband splitting passes through a zero around the strain value 1% and is relatively small, however, for larger shear strain values it increases. With the electric field applied the subband splitting keeps increasing for the whole range of the shear strain values considered. The value of the subband splitting is considerably larger as compared to the case without field. This is due to the fact that

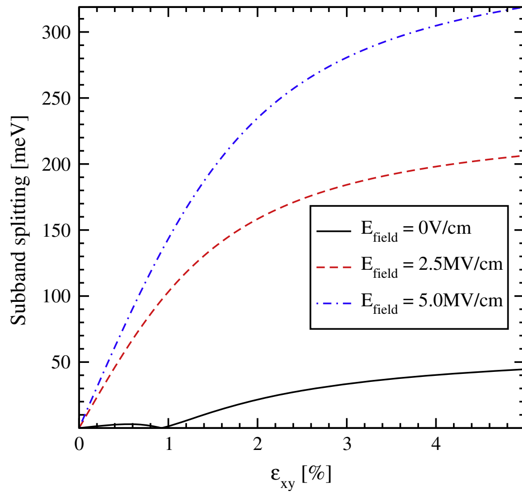

Fig. 6. Splitting of the lowest conduction subbands as a function of shear strain for different values of the electric field for $k_x = 0.25\ nm^{-1}$, $k_y = 0$, $t = 4$ nm, $\Delta E_c = 10$ eV.

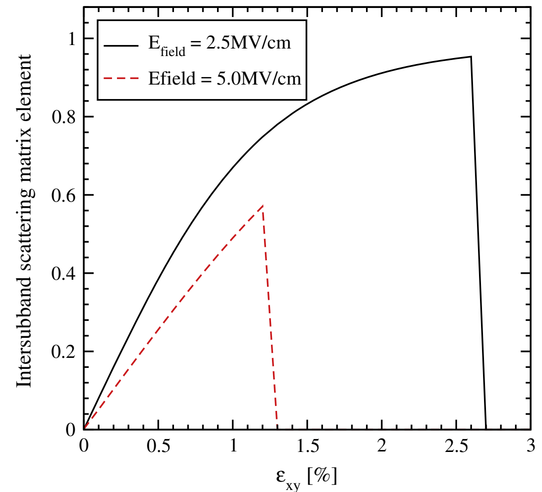

Fig. 8. Intersubband scattering matrix elements normalized to the value of the intrasubband scattering at zero strain as a function of strain for different electric field. Parameters are the same as for Fig. 7.

the electric field pushes the carriers against the interface, making them effectively more confined, which leads to the increase in splitting in energy between the lowest unprimed subbands.

The surface roughness scattering matrix elements are taken to be proportional to the product of the subband function derivatives at the interface [15]. A (001) silicon film of 4 nm thickness is considered. The surface roughness at the two interfaces is assumed to be equal and statistically independent. It is described by a mean and a correlation length [15]. Figs. 7 and 8 show the dependences on strain of the matrix elements for intrasubband and intersubband scattering normalized to the value of the intrasubband scattering at zero strain, for two values of the effective electric field. The intrasubband scattering matrix element within the lowest unprimed subband only marginally depends on shear strain. Indeed, it shows a few percent increase which becomes smaller at high shear strain, where it starts approaching unity again. This is expected in the limit of high stress. In this limit both valleys merge at the common minimum in the X point and the band dispersion is well described by a parabolic approximation [9]. Thus the lowest subband energy and the intrasubband scattering matrix element must approach their respective values in unstrained film where the dispersion is also parabolic.

The intrasubband scattering matrix element in the second subband displays a slight decrease with strain increased, which saturates at high strain. In the high strain limit the second subband, which was equivalent to the first unprimed subbands in the unstrained film, transforms into the second subband of the triangular well potential. Thus the carriers are located effectively further away from the interface. This reduces the value of the intrasubband scattering matrix elements as compared to the unstrained case, in agreement with Fig. 7. The dependence on the electric field is explained by a slight reduction of the derivative of the wave function at the interface due to its stronger penetration under the potential barrier for higher effective fields.

As shown in Fig. 8, the intersubband matrix scattering element is zero in an unstrained film, in agreement with the general rule that elastic scattering does not produce transitions between the equivalent subbands originating from the opposite equivalent valleys [16]. Shear strain lifts the subband degeneracy and thus results in a sensible intersubband scattering. Because of the subband splitting, the intersubband scattering depends strongly on the kinetic energy within the lowest subband: if the kinetic

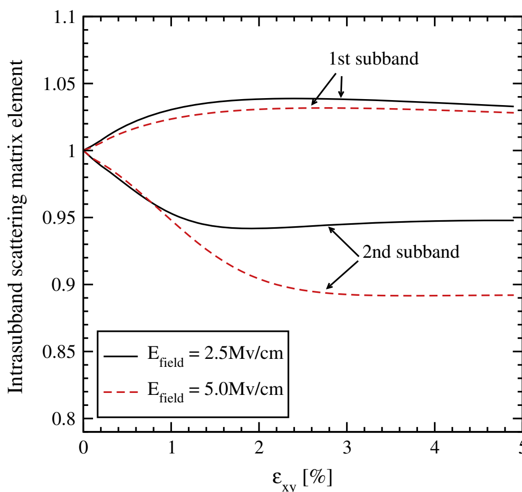

Fig. 7. Intrasubband scattering matrix elements normalized by their values for zero strain as function of shear strain for different electric field for $k_x = 0.95\ nm^{-1}$, $k_y = 0$, $t = 4$ nm, $\Delta E_c = 10$ eV.

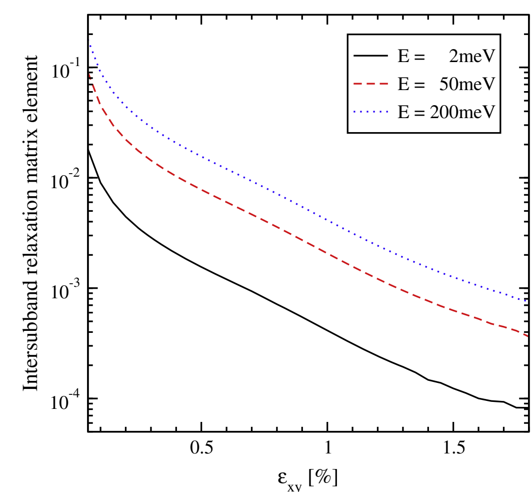

Fig. 9. Intersubband spin relaxation matrix elements normalized to intrasubband scattering at zero strain dependence on shear strain for several values of the kinetic electron energy in the subband for $k_y = 0$, $t = 4$ nm, $\Delta E_c = 10$ eV.

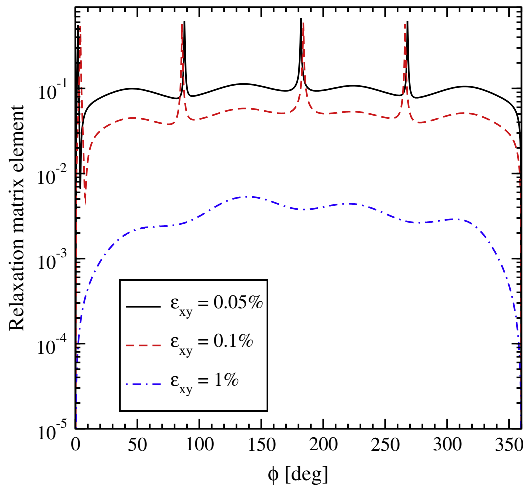

Fig. 10. Dependence of the normalized spin relaxation matrix elements on the angle between the incident and the relaxed wave for different values of strain for $k_x = 0.8\ \text{nm}^{-1}$, $k_y = 0$, $t = 4$ nm, $\Delta E_c = 10$ eV.

energy becomes lower than the subband splitting, the scattering vanishes. The intersubband splitting is larger at stronger effective electric fields, therefore, the intersubband scattering is suppressed already at weaker strain provided the kinetic energy within the subband is the same, in agreement with Fig. 8.

We now discuss the matrix elements mixing up- and down-spin states and their responsibility for the spin relaxation. The mixing depends on the strength of the spin–orbit interaction as well as on the wave vectors k_x, k_y and thus the kinetic energy within the subband. The dependence of the intersubband spin relaxation matrix element mixing the up- and down-spin states from the two different subbands is shown in (Fig. 9) in the case, when the two wave vectors before and after collision are anti-parallel and aligned along the x axis. The spin relaxation value decreases rapidly with increasing strain due to the intersubband splitting increase with strain. As soon as the intersubband splitting becomes larger than the spin–orbit interaction strength characterized by $\Delta_{so}\sqrt{k_x^2+k_y^2}$, the mixing of up- and down-spin states caused by this spin–orbit interaction is reduced.

The splitting between the subbands depends on $D\varepsilon_{xy} - k_xk_y/M$ and their degeneracy is lifted by the kinetic-like term k_xk_y/M even without shear strain. This results in a strong dependence of the surface roughness induced spin relaxation matrix elements on the angle between the incident and outgoing wave vectors. Fig. 10 shows the dependences of the relaxation matrix elements on this angle for different values of shear strain and energy of the wave. However, as follows from Fig. 10, shear strain leads to the reduction of the spin relaxation matrix element in a good agreement with Fig. 9.

4. Conclusion

We have investigated the lowest unprimed electron subband splitting in a SOI film in a wide range of parameters, including the film thickness, the shear strain, the potential barrier at the interface, and the effective electric field value. We have included the spin–orbit interaction effects into the effective low-energy **k** · **p** Hamiltonian to investigate the surface roughness induced spin relaxation. We have demonstrated that, due to the intersubband splitting increase, the matrix elements for the inter subband spin relaxation decrease rapidly with shear strain. Thus, shear strain used to enhance electron mobility can also be used to boost spin lifetime.

This work is supported by the European Research Council through the Grant #247056 MOSILSPIN.

References

[1] Huang B, Monsma DJ, Appelbaum I. Coherent spin transport through a 350 micron thick silicon wafer. Phys Rev Lett 2007;99:177209.
[2] Dash SP, Sharma S, Patel RS, de Jong MP, Jansen R. Electrical creation of spin polarization in silicon at room temperature. Nature 2009;462:491–4.
[3] Li CH, Van't Erve OMJ, Jonker BT. Electrical injection and detection of spin accumulation in silicon at 500 K with magnetic metal/silicon dioxide contacts. Nat Commun 2011;2:245.
[4] Li J, Appelbaum I. Modeling spin transport in electrostatically-gated lateral-channel silicon devices: role of interfacial spin relaxation. Phys Rev B 2011;84:165318.
[5] Li J, Appelbaum I. Lateral spin transport through bulk silicon. Appl Phys Lett 2012;100:162408.
[6] Li P, Dery H. Spin–orbit symmetries of conduction electrons in silicon. Phys Rev Lett 2011;107:107203.
[7] Song Y, Dery H. Analysis of phonon-induced spin relaxation processes in silicon 2012. arXiv:1201.6660v1 [cond-mat.mtrl-sci].
[8] Bir GL, Pikus GE. Symmetry and strain-induced effects in semiconductors. New York/Toronto: J. Wiley & Sons; 1974.
[9] Sverdlov V. Strain-induced effects in advanced MOSFETs. Springer; 2011.
[10] Cheng JL, Wu MW, Fabian J. Theory of the spin relaxation of conduction electrons in silicon. Phys Rev Lett 2010;104:016601.
[11] Ungersboeck E, Dhar S, Karlowatz G, Sverdlov V, Kosina H, Selberherr S. The effect of general strain on the band structure and electron mobility of silicon. IEEE Trans Electron Dev 2007;54(9):2183–90.
[12] Karner M, Gehring A, Holzer S, Pourfath M, Wagner M, Gös W, et al. A multipurpose Schrödinger-Poisson solver for TCAD applications. J Comput Electron 2007;6:179–82.
[13] Sverdlov V, Baumgartner O, Windbacher T, Selberherr S. Modeling of modern MOSFETs with strain. J Comput Electron 2009;8:3–4.
[14] Friesen M, Chutia S, Tahan C, Coppersmith SN. Valley splitting theory of SiGe/Si/SiGe quantum wells. Phys Rev B 2007;75:115318.
[15] Fischetti MV, Ren Z, Solomon PM, Yang M, Rim K. Six-band $k \cdot p$ calculation of the hole mobility in silicon inversion layers: Dependence on surface orientation, strain, and silicon thickness. J Appl Phys 2003;94:1079.
[16] Jin S, Fischetti MV, Tang T. Modeling of electron mobility in gated silicon nanowires at room temperature: surface roughness scattering, dielectric scattering, and band nonparabolicity. J Appl Phys 2007;102:083715.